The Journal of Experimental Biology 213, 1309-1319

doi:10.1242/jeb.039230

Hydrodynamic sensing does not facilitate active drag reduction in the golden shiner (*Notemigonus crysoleucas*)

M. J. McHenry[1,*], K. B. Michel[2], W. Stewart[1] and U. K. Müller[3]

[1]Department of Ecology and Evolutionary Biology, 321 Steinhaus Hall, University of California, Irvine, CA 92697-2525, USA, [2]Department of Marine Biology, University of Groningen, PO Box 14, 9750 AA Haren (Gn), The Netherlands and [3]Department of Biology, 2555 E San Ramon Avenue, California State University, Fresno, CA 93740, USA

*Author for correspondence (mmchenry@uci.edu)

Accepted 23 December 2009

SUMMARY

The lateral line system detects water flow, which allows fish to orient their swimming with respect to hydrodynamic cues. However, it is unclear whether this sense plays a role in the control of propulsion. Hydrodynamic theory suggests that fish could reduce drag by coordinating the motion of the head relative to detected flow signals. To test this hypothesis, we performed measurements of undulatory kinematics during steady swimming in the golden shiner (*Notemigonus crysoleucas*) at three speeds (4.5, 11.0 and 22.0 cm s^{-1}). We found that the phase shift between yaw angle and lateral velocity (20.5±13.1 deg., *N*=5) was significantly greater than the theoretical optimum (0 deg.) and the amplitude of these variables created a hydrodynamic index (*H*=0.05±0.03, *N*=6) that was less than an order of magnitude below the theoretical prediction. Furthermore, we repeated these measurements after pharmacologically ablating the lateral line hair cells and found that drag reduction was not adversely influenced by disabling the lateral line system. Therefore, flow sensing does not facilitate active drag reduction. However, we discovered that ablating the lateral line causes the envelope of lateral displacement to nearly double at the envelope's most narrow point for swimming at 4.5 cm s^{-1}. Therefore, fish may use hydrodynamic sensing to modulate the lateral amplitude of slow undulatory swimming, which could allow rapid responses to changes in environmental flow.

Key words: undulation, locomotion, hydrodynamics, hair cells, lateral line.

INTRODUCTION

Fish use a number of sensory systems to stabilize their body orientation and to direct their swimming. To stabilize during swimming, fish use the vestibular organ to respond to linear and rotational accelerations to help counter perturbations from self-generated and environmental flows (Platt, 1988). To direct their swimming, fish use visual, olfactory and acoustic cues (Collin and Shand, 2003; Ladich and Bass, 2003; Valentincic, 2004), as well as hydrodynamic signals detected by their lateral line (Bleckmann, 1994; Coombs and Montgomery, 1999). For example, adult fish sense the pressure field generated by swimming prey in the dark (Coombs and Conley, 1997; Coombs et al., 1996) and the flow of a suction feeding predator triggers a startle response in larval fish (McHenry et al., 2009). However, it is unclear whether fish use flow sensing in the control of undulatory propulsion. Investigators have long speculated that flow may be detected to enhance hydrodynamic performance or to respond to changes in the environment (reviewed by Dijkgraaf, 1963). Here we present an experimental test of the role of the lateral line system in the control of steady swimming in a teleost fish, the golden shiner (*Notemigonus crysoleucas*).

There is a growing body of experimental evidence suggesting that the lateral line system influences how a fish swims. Aeronautical research has demonstrated that thrust generation by a fin-like robotic foil is more efficient when its motion is coordinated with ambient vortices (Gopalkrishnan et al., 1994). Trout (*Oncorhynchus mykiss*) capitalize on such advantages by entraining their undulatory swimming within the wake of a cylinder (Liao et al., 2003a; Liao et al., 2003b). This entrained swimming, called the Kàrmàn gait, is altered when the lateral line system is pharmacologically ablated (Liao, 2006). The same treatment causes lamprey (*Petromyzon marinus*) swimming in still water to use a slightly greater undulatory wavelength (Ayali et al., 2009). These studies demonstrate that swimming may be altered by disabling the lateral line, but it remains unclear what performance advantages come from using flow sensing to mediate steady swimming.

Hydrodynamic theory demonstrates a possible role for the lateral line in drag reduction (Lighthill, 1995). According to one model (Lighthill, 1993), drag should be reduced by minimizing the pressure difference [$\Delta p(t)$, where t is time] between the lateral surfaces of the head. Through an application of potential flow theory, this quantity is shown to be equal to the difference between components generated by the yaw [$\Delta p(t)_{\text{yaw}}$] and translation [$\Delta p(t)_{\text{trans}}$] of the head according to the following equations (Lighthill, 1993):

$$\Delta p(t) = \Delta p(t)_{\text{trans}} - \Delta p(t)_{\text{yaw}} , \quad (1)$$

where

$$\Delta p(t)_{\text{trans}} = 2b(1 + k_1)\rho V''(t) , \quad (2)$$

$$\Delta p(t)_{\text{yaw}} = 2b(k_1 + k_2)\rho U(t)\alpha'(t) , \quad (3)$$

b is half the width of the head, ρ is the density of water, V'' is the lateral acceleration of the head, U is the swimming speed, α' is yaw rate (in rad s^{-1}), and k_1 and k_2 are numerical constants that depend on the shape of the head. The pressure difference, and therefore drag, is minimized when these two components vary synchronously with an equal magnitude (Lighthill, 1993). This occurs in steady swimming when the yaw angle oscillates in phase with lateral

velocity. The components of the pressure difference maintain an equal magnitude when the following ratio, the hydrodynamic index H, is constant across swimming speeds:

$$H = \frac{U\alpha_{amp}}{V_{amp}} , \quad (4)$$

where α_{amp} and V_{amp} are the amplitudes of yaw angle and lateral velocity, respectively. Under optimal conditions for minimizing drag, the hydrodynamic index may be predicted from morphometrics of head shape according to the following equation (Lighthill, 1993):

$$H_{morph} = \frac{1 + k_1}{k_2 + k_1} . \quad (5)$$

Agreement between kinematic measurements of the hydrodynamic index and its prediction from morphology have been reported for herring (Rowe et al., 1993). Lighthill argued that such motion is best achieved by sensory feedback from the lateral line system. It was predicted that an absence of this feedback should generate a phase shift of 90 deg. between yaw angle and lateral velocity, rather than the optimum of 0 deg. (Lighthill, 1995). Furthermore, the hydrodynamic index should not match that predicted from morphometrics in swimming without the lateral line. In the present study, we tested this active drag reduction hypothesis (Lighthill, 1995) by measuring the head kinematics of the golden shiner. We also tested whether this species deviates from optimal kinematics when they do not receive sensory feedback from their lateral line. To this end, we ablated the lateral line hair cells by exposing them to an ototoxic antibiotic.

Our experiments focused on the golden shiner because it is a species that swims steadily and possesses a lateral line morphology that is typical of a broad diversity of teleost species (Fig. 1A). This North American freshwater cypriniform readily holds station when exposed to flow, such as in a flow chamber. This is an ideal behavior because many of the above-mentioned advantages of drag reduction should be most apparent in steady undulatory swimming. Furthermore, the lateral line morphology of this species includes

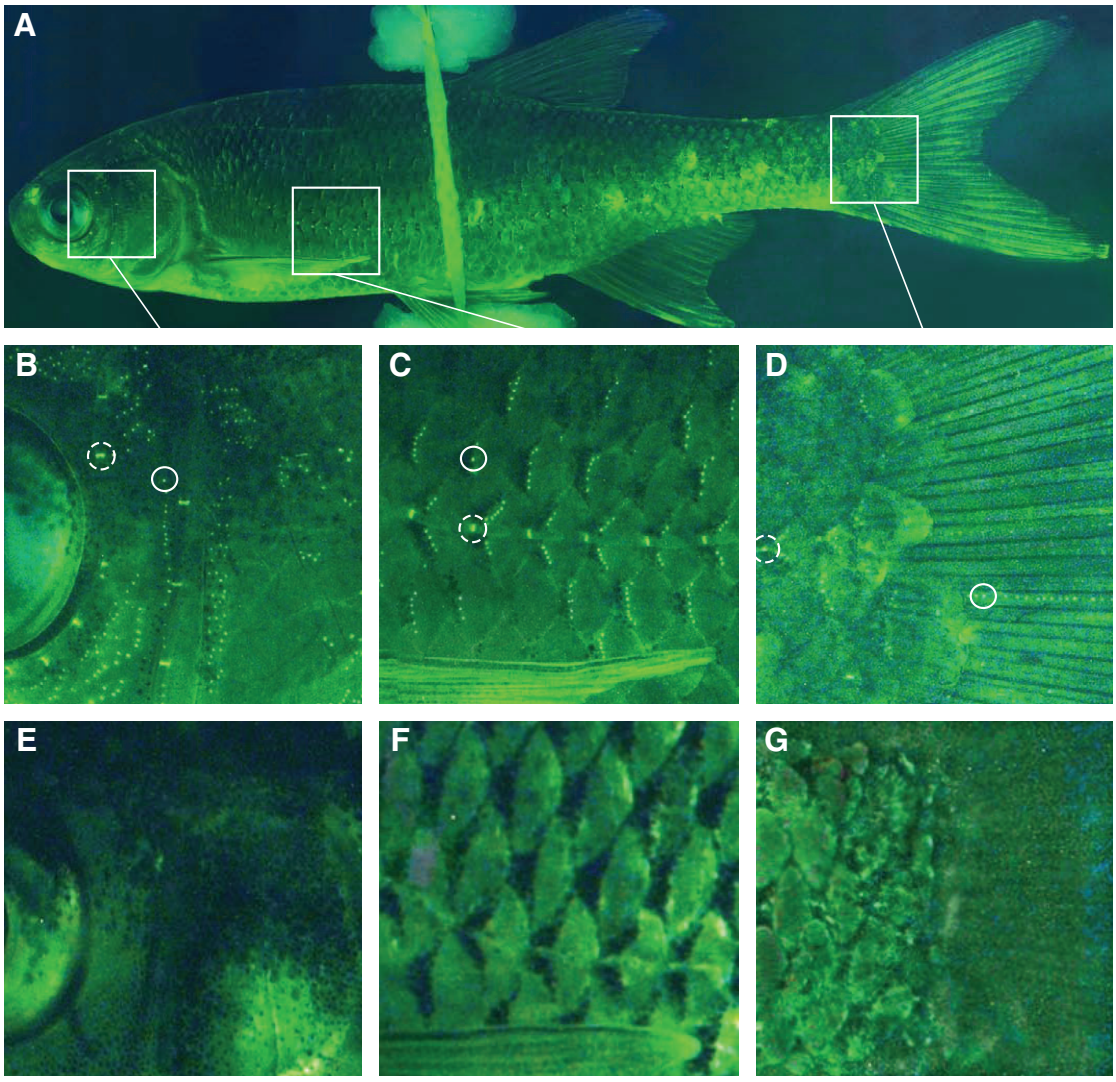

Fig. 1. The lateral line system of the golden shiner *Notemigonus crysoleucas*. (A) A composite image of multiple photographs of the lateral surface of an individual stained with DASPEI under epifluorescent illumination. (B–D) Details of the same image reveal individual neuromasts as light circles in the cranial (B), trunk (C) and caudal (D) regions with canal (dashed circle) and superficial (circle) neuromasts highlighted. (E–G) These images for the same regions of the body with the same stain and illumination in a different individual are shown after treatment with neomycin sulfate (see text for details). Neuromasts are not visible in these panels because the hair cells have been pharmacologically ablated.

both superficial and canal neuromasts throughout the head (Fig. 1B) and trunk (Fig. 1C), and the caudal fin includes superficial neuromasts between the fin rays (Fig. 1D). Therefore, flow is detected by this species over the entire length of its body.

MATERIALS AND METHODS

Animals and lateral line ablation

Golden shiners, *Notemigonus crysoleucas* Mitchill 1814 (total length between 9 and 11 cm), were obtained from a commercial fish farm (Alpine Fishery, Alpine, CA, USA). They were kept in clean and well-oxygenated fresh water at 19°C on a 12 h/12 h light–dark cycle and were fed regularly. During experiments, fish were handled carefully to avoid damage to the lateral line system. Individuals were permitted to habituate to flow for at least 30 min before experiments were conducted. Measurements began within 1 h of treatment and were completed within 2 h.

We pharmacologically ablated the lateral line system with an aminoglycoside antibiotic to evaluate its influence on swimming. This class of antibiotics disables hair cells by inducing apoptosis (Williams et al., 1987) or blocking the mechanotransduction channels (Kroese et al., 1989). We developed a protocol for ablating the lateral line system with the antibiotic neomycin sulfate in this species. A previous study on larval zebrafish found that a 500 μmol l^{-1} dose of neomycin sulfate successfully eliminates lateral line hair cells when exposed for 1 h (Harris et al., 2003). However, following this treatment, we found that adult shiners still initiated swimming in response to a jet of water (see Liao, 2006) administered with a 5 ml disposable transfer pipette. Furthermore, the lateral line hair cells of these treated fish were still visible (as in Fig. 1A–D) when stained with the fluorescent dye DASEPI {2-[4-(dimethylamino)styryl]-*N*-ethylpyridinium iodide; Molecular Probes, Eugene, OR, USA} (Fig. 1B–G) and observed with a stereomicroscope (Zeiss Discovery V.20 with GFP filter set and an AxioCam HRc camera, Carl Zeiss, Thornwood, NY, USA). This voltage-sensitive dye indicates the presence of functioning lateral line hair cells (Murakami et al., 2003). Increasing the exposure duration to 2 h and 4 h showed no effect on the response to the fluid jet. A 6 h treatment created a reduction in the responsiveness to the jet, but fish still responded to this stimulus. We therefore extended the exposure to 24 h [typical of treatments using other aminoglycoside antibiotics (Blaxter and Fuiman, 1989; Montgomery et al., 1997)] and found that this longer treatment caused fish to cease responding to the fluid jet and that lateral line hair cells were no longer visible when stained with DASPEI (e.g. Fig. 1E–G). After this treatment, fish were capable of responding to an acoustic stimulus and maintained equilibrium, which indicated that neomycin exposure did not disable the inner ear hair cells. A sham treatment was performed on a separate group of fish by placing them in a treatment tank for 24 h without the addition of neomycin sulfate.

Video recording of swimming

We recorded the kinematics of steady swimming in fish before and after ablating the lateral line system. The kinematics of swimming were recorded with high speed videography (250 frames s^{-1}, with 1024×1024 pixels of spatial resolution, Photron Fastcam 1024, Photron USA, San Diego, CA, USA) in a flow tank. This swimming occurred within a transparent working section of the flow tank (30.5 cm long, 10.2 cm wide and 11.4 cm deep). Laminar flow was created by a series of flow straighteners and a 130 μm nylon filter. A mirror oriented with a 45 deg. angle below the working section allowed for simultaneous viewing of fish from lateral and ventral perspectives. The camera focused on the ventral view and the side view was monitored during recordings to ensure that fish maintained a center-height position. Fish were back-lit with LED and halogen lights positioned behind a diffuser to enhance contrast. They were recorded at three flow speeds (4.5, 11.0 and 22.0 cm s^{-1}) that were calibrated from recordings of dye plumes injected at positions throughout the cross-section of the working section. Water chemistry and temperature in the flow tank were equivalent to those in the holding tanks. These recordings were performed on 7 fish treated with neomycin and on 3 fish in sham experiments.

Swimming kinematics

Coordinates for the midline of the head and body of the fish were acquired by analyzing our video recordings with customized software (Fig. 2A). This program and all other software developed for this study were created with Matlab (v.2009a, with the image processing toolbox, MathWorks, Natick, MA, USA). The program first distinguished the body of the fish from its surroundings by thresholding the pixel values of the video frame (Russ, 1999). This created a binary image where the fish's body is differentiated as white pixels on a black background (Fig. 2B). The anterior-most point on the head was identified as the left margin of white pixels on the video frame (Fig. 2A). Starting at this point, the program found coordinates along the anterior periphery on the left and right sides of the head, until reaching the length of the cranium, which was measured independently. A smoothed cubic spline was fitted to these coordinates and the program identified the tip of the rostrum as the point of greatest curvature along this spline (Fig. 2C). The base of the cranium was calculated as the mean coordinate between the posterior edges of the traced periphery (Fig. 2B). Coordinates describing the midline of the body were acquired with an algorithm that iteratively moved down the body, starting at the head. For each iteration, pixel intensity values were determined along an ellipse with its center at the previous point (Fig. 2D). The edges of the body were identified by normalizing pixel values by their range. The location of the edges was well approximated by pixels having a relative intensity of 0.4 (Fig. 2E) and a midline center point was defined as the mean coordinate between these edges. These iterations ceased upon reaching the body length and we used a linear interpolation to define the acquired coordinates at an equal interval along the body (Fig. 2A).

Post-processing of the coordinate data was used to identify the undulatory wave of bending. To remove high-frequency noise created by digitizing error, we filtered each time series of coordinates with a second-order low-pass Butterworth filter. We used a cutoff frequency of 30 Hz, which lies approximately an order of magnitude above the tail-beat frequency and corresponds to one-quarter of the Nyquist frequency (125 Hz). From each recording, we analyzed between 7 and 9 tail beats and over this duration fish would commonly drift laterally across the working section. In order to remove this relatively slow motion from our analysis, we passed the coordinate data through a high-pass filter (second-order Butterworth) with a cut-off frequency of 0.3 Hz. This frequency was about an order of magnitude below the tail-beat frequency and therefore did not substantially alter the amplitude of oscillations within a tail-beat period. In order to locate the undulatory wave, we fitted a cubic spline to body coordinates as a function of body position. The wave peak was identified as the position where the trend in lateral position changed from increasing to decreasing in magnitude (i.e. the zero-point of the first derivative of the cubic spline) in the posterior half of the body.

Parameters describing undulatory kinematics were calculated from the acquired coordinates. The speed of an undulatory wave

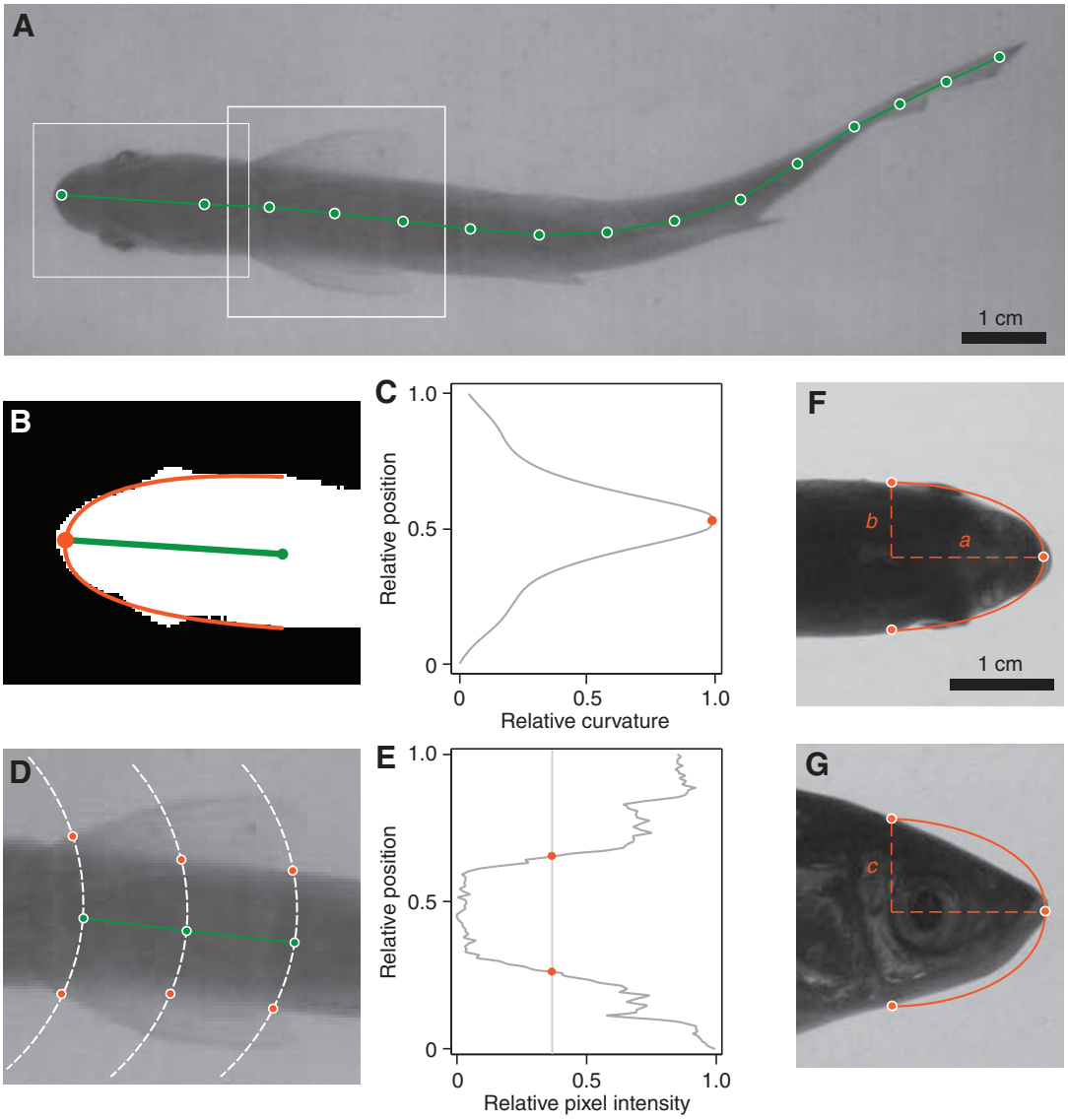

Fig. 2. The acquisition of kinematic and morphometric data. (A) An individual video frame from a recording of a swimming fish from a dorsal perspective displays the midline coordinates (green circles and lines) found by the customized software developed for the present study. White boarders denote the locations of panels B and D. (B) The coordinates for the head were found by transforming the 8-bit grayscale video frame into a binary image with a user-defined threshold pixel value. A smoothing cubic spline (orange line) traced the anterior margin of the head. The center between the posterior margin of these points (green circle) defined the base of the head and the rostrum (orange circle) was determined from (C) the point of maximum curvature (orange circle) along the cubic spline (orange line in B). (D) Midline coordinates posterior to the cranium (green circles) were calculated as the mean position between lateral margins (orange circles), found from pixel values along a semi-ellipse (dashed line). (E) The pixel values along the ellipses (values for the middle ellipse in D shown) indicate the location of the body margins (orange circles) at a relative pixel intensity of 0.4. (F and G) The anterior region of the head was approximated as an ellipsoid (orange line) from measurements for half the head length (*a*), width (*b*) and height (*c*), from three landmarks (orange circles) selected from digital photographs. These landmarks included the dorso-ventral (F) and lateral (G) margins of the head at the posterior margins of the eyes and the anterior margin of the premaxilla.

was calculated from a linear least-squares curve fit to the position of the wave peak as a function of time. The undulatory wave length was calculated as the ratio of wave speed and the tail-beat frequency (measured from head kinematics). For each sequence, we measured the range of lateral excursion for all body positions over the tail-beat period. The amplitude envelope for the lateral position of the body was calculated as the mean of these range values. The yaw angle was calculated from the filtered coordinates of the head and rostrum (Fig. 2B,C). Measurements of the amplitude, frequency and phase of the head position were found by non-linear least-squares curve fits of sine waves to measurements of both lateral position and yaw angle.

Head morphometrics

Potential flow theory may be formulated to predict optimal kinematics of the head to its shape (Lighthill, 1993). This model approximates the head as a hemiellipsoid with dimensions that we measured from landmarks taken from high-contrast photographs (using a Canon EOS 350D, Canon Inc., Tokyo, Japan) of dead fish (N=7) that were backlit with a white light and diffuser. These landmarks consisted of the lateral and dorso-ventral margins of the head at the posterior margins of the eyes and the anterior margin of the premaxilla (orange circles in Fig. 2F,G). From these coordinates, head shape was described by the length of the head (*a*, Fig. 2F), the minor lateral axis (*b*, one-half the head width, Fig. 2F)

and the minor vertical axis (c, one-half the head height, Fig. 2G). The model relates these dimensions to the kinematics of the head through the calculation of two numerical constants, k_1 and k_2 (Eqns 2, 3 and 5), defined by the following equations [from equations A26, A29, A32 and A40 in Lighthill (Lighthill, 1993)]:

$$k_1 = \frac{\beta_0}{2-\beta_0}\ , \tag{6}$$

where

$$\beta_0 = \frac{ac}{b}\int_0^{\infty}\frac{d\lambda}{\left(\left(\frac{a}{b}\right)^2+\lambda\right)^{1/2}(1+\lambda)^{3/2}\left(\left(\frac{c}{b}\right)^2+\lambda\right)^{1/2}}\ , \tag{7}$$

and

$$k_2 = \frac{\left(\left(\frac{a}{b}\right)^2-1\right)(\beta_0-\alpha_0)}{2\left(\left(\frac{a}{b}\right)^2-1\right)-\left(\left(\frac{a}{b}\right)^2+1\right)(\beta_0-\alpha_0)}, \tag{8}$$

where

$$\alpha_0 = \frac{ac}{b}\int_0^{\infty}\frac{d\lambda}{\left(\left(\frac{a}{b}\right)^2+\lambda\right)^{3/2}(1+\lambda)^{1/2}\left(\frac{c}{b}+\lambda\right)^{1/2}}\ . \tag{9}$$

In Eqns 7 and 9, λ is the position along an ellipsoid, over which the integration occurs. Using our measurements for a, b and c, we solved for k_1 and k_2 numerically using Mathematica 6.0 (Wolfram Research Inc., Champaign, IL, USA). As a test of the model, we compared our prediction for the hydrodynamic index from these morphometrics (Eqn 5) with that calculated from kinematics (Eqn 4).

Statistical analysis

Analysis of variance (ANOVA) tests were used to determine the effects of lateral line ablation, swimming speed and individual differences on kinematics and hydrodynamics. The contributions of these factors were considered with a 3-factor ANOVA with the individual and treatment (before and after lateral line ablation) as categorical variables and speed used as a continuous independent variable. The dependent variables in these tests consisted of the parameters describing the undulatory kinematics, the kinematics of the head, and the predicted pressure differences for the head. Categorizing measurements by individual allowed paired comparisons for the effects of treatment and speed. 95% confidence intervals among individuals for each treatment group and speed permitted *post-hoc* comparisons for the effects of these factors.

RESULTS

Undulatory kinematics

We found that the golden shiner exhibits undulatory kinematics that are common for a subcarangiform swimmer (Bainbridge, 1963; Videler and Hess, 1984). For the present species, we found that this motion is well described by the following equation:

$$y(s,t) = y_{amp}(s)\sin(2\pi f(ws - t))\ , \tag{10}$$

where w is the undulatory wave speed, s is the relative body position and f is the tail-beat frequency. The amplitude envelope, $y_{amp}(s)$, is given by the following:

$$y_{amp}(s) = c_1(s-c_2)^2 + c_3\ , \tag{11}$$

where c_1 is the amplitude growth rate (units of BL^{-1}, where BL is body lengths), c_2 is the position of minimum lateral excursion (in BL), and c_3 is the minimum lateral excursion (in BL). This equation provided a uniformly excellent fit (R^2>0.90) to measurements of midline coordinates. As a means of structuring our consideration of undulatory swimming, we examined how swimming speed and lateral line ablation affected the parameters in these equations.

The speed and length of the undulatory wave did not vary with swimming speed and neither measure was affected by ablating the lateral line system. The peak of the undulatory wave propagated down the posterior half of the body at a nearly constant rate (Fig. 3A,B) and did not vary significantly with swimming speed. We also found no significant differences in wave speed between swimming before and after lateral line ablation (Fig. 3C; Table 1). The undulatory wave length, L (L=w/f; f was measured from the kinematics of the head, described below), also did not vary significantly with swimming speed or change significantly after lateral line ablation (Fig. 3D). Across the tested speed range and prior to the ablation, golden shiners swam with a mean (±1 s.d.) wave speed of 2.27±0.25 BL s^{-1} and a wave length of 0.58±0.12 BL (N=4 for 4.5 cm s^{-1} and N=6 for 11.0 and 22.0 cm s^{-1}).

The amplitude envelope of the body varied with swimming speed and was affected by the lateral line ablation. Among the three parameters describing lateral excursion (Eqn 11), the minimum amplitude along the length of the body (c_3) most commonly varied among our measurements. Minimum amplitude increased significantly with speed before ablation of the lateral line (Fig. 4F; Table 1). Furthermore, the ablation caused fish to nearly double their minimum amplitude (from 0.0085±0.0036 BL, N=4, to 0.0153±0.0022 BL, N=6) when swimming at 4.5 cm s^{-1}. This effect was apparent in individual sequences (Fig. 4A) and as a general trend among all individuals (Fig. 4B). As a consequence of the elevated lateral excursion in swimming after ablation, the tail-beat amplitude increased nearly 60% after the ablation (from 0.0588±0.0057 BL, N=4 to 0.0936±0.0147 BL, N=6; Fig. 4F) for swimming at 4.5 cm s^{-1}. In contrast, the lateral line ablation did not cause lateral excursion to increase significantly at higher speeds (Fig. 4C–F; Table 1).

We performed sham experiments to evaluate whether our comparisons of swimming before and after the experimental ablation could be attributed to factors other than disrupting the lateral line system. These experiments followed the same sequence of events as the ablation experiments, except for the addition of ototoxic neomycin to the treatment tank (see Materials and methods for details). We found no significant effects of the sham treatment (Table 1), which validates our interpretation of results from the lateral line ablation.

Head kinematics, morphometrics and hydrodynamics

We examined the effects of swimming speed and lateral line ablation on the kinematics of the head. Oscillations in the position of the head were well approximated by sine waves (Fig. 5A–F), which showed a high coefficient of determination when fitted to measurements of the lateral velocity and yaw angle of the head (R^2>0.85 for all sequences). From the fitted curves, we found that the frequency of these head oscillations did not vary significantly with swimming speed or lateral line ablation (Fig. 5G; Table 1). However, the phase shift between the lateral velocity and the yaw angle did change significantly with the ablation (Table 1). The phase

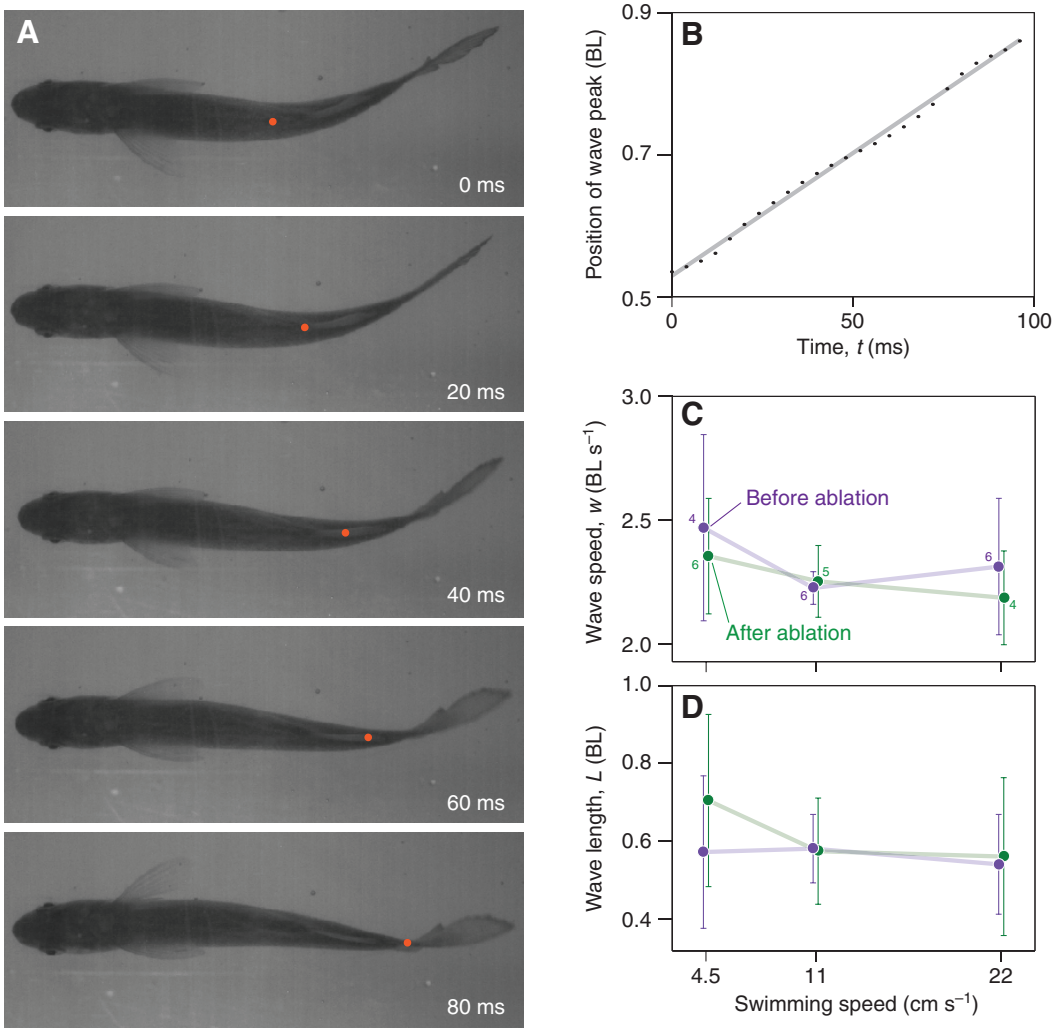

Fig. 3. The speed and length of the undulatory wave. (A) Representative video frames for a fish (body length, BL=10.2 cm) swimming at 11.0 cm s^{-1} at 20 ms intervals. Orange circles denote the position of the undulatory wave peak, identified from acquired midline coordinates (e.g. Fig. 2A) as the most lateral position in the posterior region of the body (see text for details). (B) The relative body position of this wave varies as a linear function of time. A linear least-squares curve fit (R^2=0.99) for this wave finds a speed of 3.4 BL s^{-1}. (C) Wave speed is shown for all individuals considered for three swimming speeds before (purple) and after (green) lateral line ablation (values for swimming speed are denoted in D). Mean values among individuals (accompanying numbers specify the sample sizes) and error bars indicating 95% confidence intervals are shown. (D) The wave length was calculated as the ratio of wave speed and the tail-beat frequency (Fig. 5G).

shift increased with speed prior to ablation, but decreased with speed after ablation (Fig. 5H). Despite this change, the mean phase shift after the ablation (31.5±18.5 deg., N=5) was not substantially different from that before the ablation (20.5±13.1 deg., N=5 for 4.5 cm s^{-1} and N=7 for 11.0 and 22.0 cm s^{-1}). In contrast, the amplitudes of lateral velocity and yaw angle were significantly altered by the lateral line ablation (Table 1). This effect was most apparent at a swimming speed of 4.5 cm s^{-1}, where there was approximately a 3-fold increase in the amplitude of both lateral velocity (from 1.11±0.33 cm s^{-1} to 3.35±0.95 cm s^{-1}, N=5; Fig. 5I) and yaw angle (from 1.41±0.98 deg. to 4.05±0.99 deg., N=5; Fig. 5J) with the treatment. Therefore, ablating the lateral line system had a more substantial effect on the amplitude than the timing of head motion.

We used potential flow theory (Lighthill, 1993) to model the pressures generated by these kinematic patterns (Eqns 1–5). For swimming at 4.5 cm s^{-1}, increases in the rates of head motion created by the lateral line ablation (Fig. 5I,J) caused an elevation in the amplitude of the pressure difference (Fig. 6). On average, there was a greater than 3-fold increase in total pressure (from 4.1±1.7 Pa, N=7 to 14.2±3.6 Pa, N=3) due to the ablation for swimming at this speed, but no such difference was observed at faster speeds

Table 1. P-values for ANOVA tests

Factor	w	L	A	c_1	c_2	c_3	f	ϕ	V_{amp}	α_{amp}	dp_{rot}	dp_{trans}	H
Treatment (d.f.=1)	0.79	0.33	0.13	0.27	0.40	**<0.001**	0.31	**<0.01**	**<0.01**	**<0.001**	0.35	0.21	**<0.01**
Speed (d.f.=1)	0.57	0.06	0.07*	0.10*	0.22	**<0.01***	0.11	0.20	**0.02***	**0.05***	**<0.001***	0.08	**0.02**
Individual (d.f.=6)	0.66	0.01	0.08	0.24	**<0.01**	0.86	0.10	0.82	0.45	0.12	0.27	0.69	**0.31**
Treatment × speed (d.f.=1)	0.58	0.37	0.48	0.90	0.69	**<0.01**	0.56	0.07	0.07	**<0.01**	0.18	0.49	**0.01**
Experiment × individual (d.f.=6)	0.83	0.31	0.23	**0.03**	**<0.01**	**0.04**	0.30	0.27	0.12	0.08	**0.04**	0.44	0.39
Speed × individual (d.f.=6)	0.69	**0.04**	0.06	0.23	0.07	0.51	0.69	0.16	0.93	0.29	0.43	0.97	0.76

V, wave speed; L, wave length; A, tail-beat amplitude; c_1, amplitude growth rate; c_2, position of minimum lateral excursion; c_3, minimum lateral excursion; f, tail-beat frequency; ϕ phase shift between lateral velocity and yaw angle; V_{amp}, amplitude of lateral velocity; α_{amp}, amplitude of yaw angle; dp_{rot}, pressure difference from rotation; dp_{trans}, pressure difference from translation; H, hydrodynamic index.
Significant values at the P≤0.05 level are highlighted in bold. *In sham experiments, P≤0.05 (N=3) for this category.

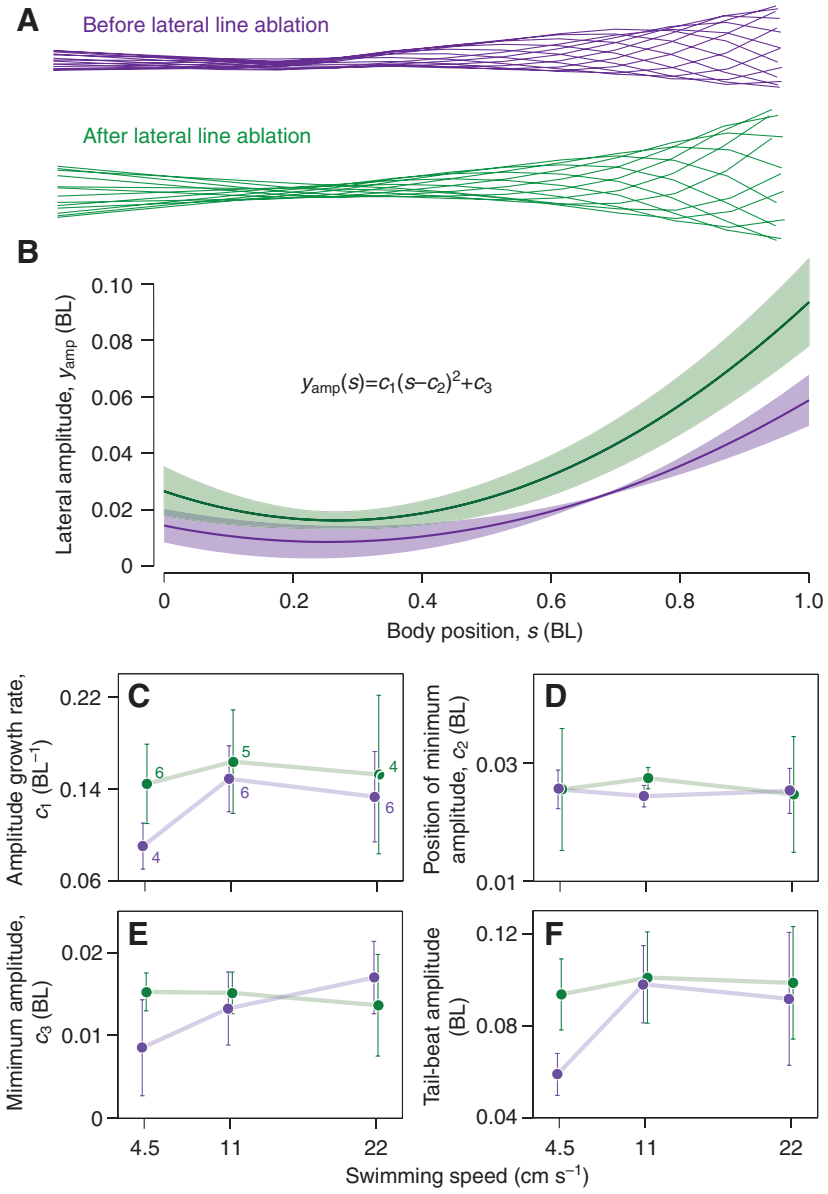

Fig. 4. The amplitude envelope of undulatory kinematics. (A) Representative midlines traced for a single tail beat are shown for an individual (BL=10.5 cm) swimming at 4.5 cm s^{-1} before (purple lines) and after (green lines) lateral line ablation. (B) The amplitude envelope is expressed by Eqn 11 (reprinted in this panel) with three coefficients that were found by a non-linear least-squares curve fit (see text for details). Using these coefficient values, the lateral excursion was calculated along the body for swimming before (in purple) and after (in green) lateral line ablation. The mean excursion (lines) over the length of the body is shown with 95% confidence intervals (shaded areas) for swimming at 4.5 cm s^{-1} (N=4). (C–F) The mean values (±95% confidence intervals) among individuals for four parameters that describe the amplitude envelope. The sample size for each mean value is indicated by a number next to the filled circles in panel C.

(Fig. 6G). Hydrodynamic modeling also demonstrated that the pressure difference due to yaw is substantially less than that from translation. The pressure difference due to yaw reached only 30% (±8%, N=7) of the pressure difference generated by translation at the highest swimming speed (22 cm s^{-1}, Fig. 6F, Table 1). At the lower swimming speeds, the contribution from yaw was even lower (7±2%, N=6, at 4.5 cm s^{-1} and 16±3%, N=6, at 11 cm s^{-1}). This small hydrodynamic contribution from yawing is reflected in our measurements of the hydrodynamic index. Our morphometric analysis of the head calculated a hydrodynamic index (H_{morph}, Eqn 5) of 0.65 (±0.05, N=7, Table 2). This value differs markedly from the hydrodynamic index calculated from kinematics (H, Eqn 4), which was 0.05 (±0.03, N=6, Fig. 6H) across speeds before the ablation. Hence in golden shiners with an intact lateral line system, the hydrodynamic index cannot be predicted from head morphology. After ablation, the hydrodynamic index approached the value predicted for morphometrics for swimming at 4.5 cm s^{-1} (0.94±0.29, N=3). However, this result is not consistent with the hypothesis that the lateral line system mediates kinematics to minimize the pressure difference.

DISCUSSION

The present study tested and rejected the hypothesis that fish use the lateral line system to actively minimize drag on the head in the golden shiner (Lighthill, 1993; Lighthill, 1995). Our findings instead suggest that the lateral line system contributes to the control of the lateral excursion of the body. This function could enable fish to respond rapidly to changes in environmental flow conditions.

The active drag reduction hypothesis

We tested the hypothesis that the lateral line system allows fish to actively reduce drag during swimming. This hypothesis makes four predictions, the first two of which were evaluated by kinematic recordings alone. First, a fish is predicted to rotate and translate its head to minimize pressure differences across the head, which requires that yaw angle oscillates in phase with the lateral velocity of the head (Lighthill, 1993). Contrary to this prediction, we found that the golden shiner swims with a phase shift of around 20 deg. (Fig. 5H). Second, the amplitude of oscillations in yaw angle and lateral velocity should be predictable from the shape of the head. In particular, the hydrodynamic index, H, measured from kinematics

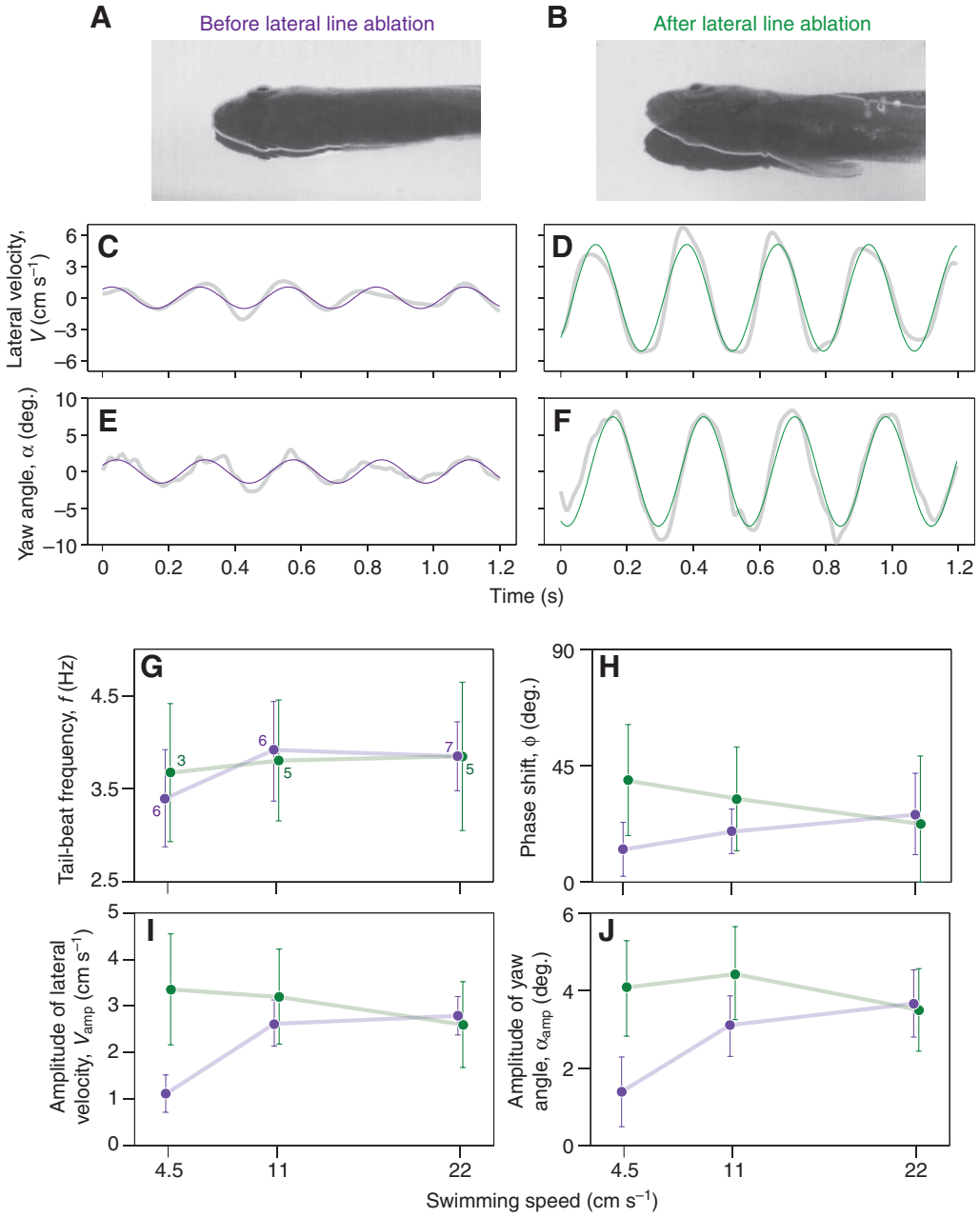

Fig. 5. The kinematics of the head during swimming. (A–F) The kinematics for a representative individual before (A, C and E) and after (B, D and F) lateral line ablation for swimming at 4.5 cm s^{-1}. (A,B) Pairs of video stills (highlighted with a 2-pixel border) of the anterior half of the body from a dorsal perspective are overlaid at the extremes of lateral excursion of the head. (C–F) Measurements (gray lines) are shown with fitted sine waves (colored lines) for the lateral velocity (C,D) and yaw angle (E,F) of the head. Kinematic parameters measured from such curve fits are shown as mean values (±95% confidence intervals) for (G) the tail-beat frequency, (H) the phase shift between the lateral velocity of the head and the yaw angle, and the amplitudes of (I) lateral velocity and (J) yaw angle for fish when they have a functioning lateral line system (purple) and after its ablation (green). The samples size for each category is denoted in panel G.

should match that calculated from the dimensions of the head, H_{morph} (Eqn 5). Counter to this prediction, we found that the hydrodynamic index of swimming was less than an order of magnitude below what was predicted from morphometrics (Fig. 6H).

The remaining two predictions of the active drag hypothesis were tested by ablating the lateral line system. The lateral line is predicted to allow a fish to operate closer to optimal kinematics than would otherwise be possible (Lighthill, 1993). The hypothesis predicts that the phase shift between yaw angle and lateral velocity should approach 90 deg. in the absence of lateral line feedback (Lighthill, 1995). Consistent with this expectation, the phase shift of the yaw angle did increase slightly for swimming at slow speed when we ablated the lateral line (Fig. 5H). However, this was a statistically insignificant change that fell well short of the prediction (Lighthill, 1995). Finally, the hypothesis predicts that the hydrodynamic index measured from kinematics should deviate from the prediction from morphometrics in the absence of lateral line feedback. In contrast, we found that ablation caused the hydrodynamic index to approach

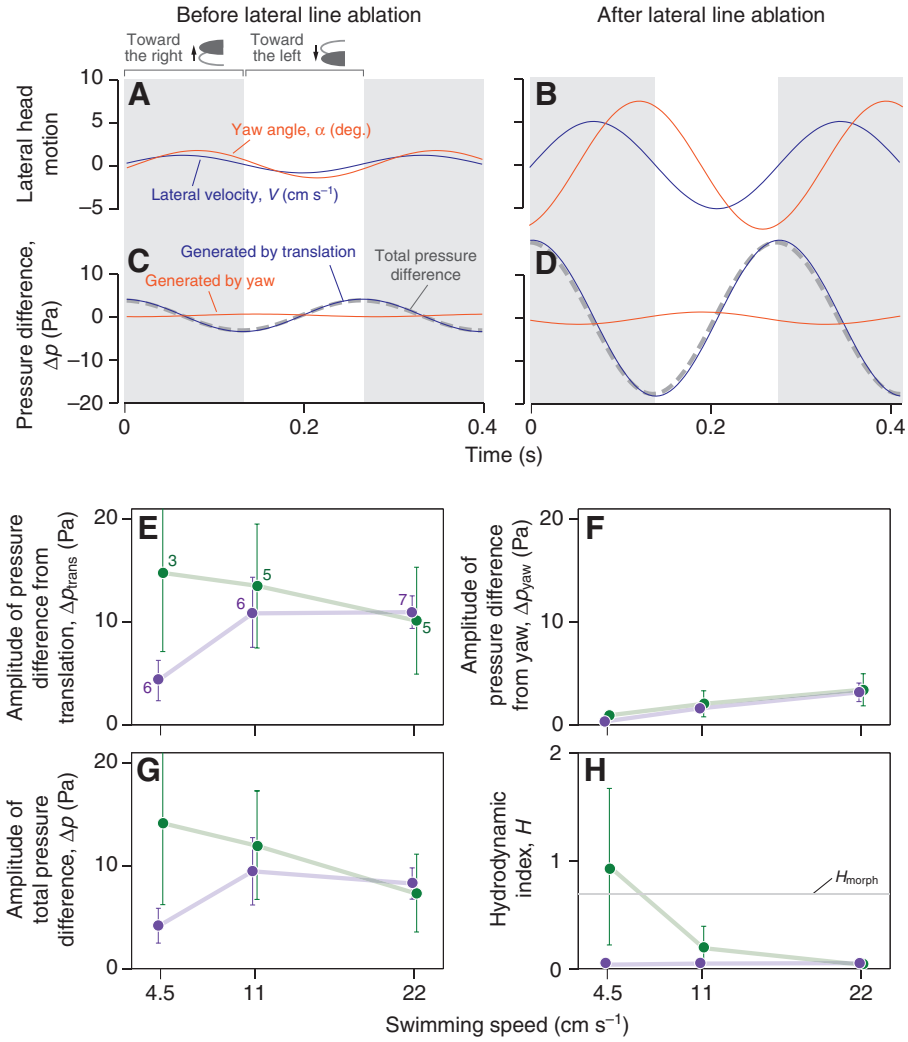

Fig. 6. The hydrodynamics of the head during swimming. (A–D) The lateral motion and resulting pressure differences across the head are shown for a representative fish from before (A and C) and after (B and D) lateral line ablation. (A,B) Oscillations in the lateral velocity (blue line) and yaw angle (orange line) from kinematics measurements (e.g. Fig. 5). These data provided the basis for estimates of the pressure differences across the head (calculated from potential flow theory, Eqn 1) generated from the translation (blue line, Eqn 2) and yawing (orange line, Eqn 3) of the head. (E–H) Mean parameter values (±95% confidence intervals) for the hydrodynamics of swimming in fish from before (green) and after (purple) lateral line ablation. (H) The hydrodynamic index (H) is shown with the value predicted (Table 2) from morphometrics (H_{morph}, gray line). The samples size for each category is denoted in panel E.

the value predicted from morphometrics (Fig. 6H) instead of deviating from it. In summary, our kinematic measurements and experimental manipulation on the golden shiner contradict all four predictions of the active drag reduction hypothesis.

These results show that the active drag reduction hypothesis cannot be considered generally valid. Previous experimental studies supported active drag reduction in some species. Using kinematic measurements similar to the present study, the time course of transient swimming in an individual herring (*Clupea harengus*) demonstrated a hydrodynamic index that was close to the morphometric prediction and a review of prior studies found similar agreement in single swimming sequences in 2 out of 4 species considered (Rowe et al., 1993). Although the present study offers a more comprehensive test of the drag reduction hypothesis by considering numerous individuals and an experimental manipulation, it remains possible that herring are unique in their ability to use the lateral line to control head motion. Herring and other clupeid fishes possess a unique subcerebral canal system that is highly sensitive to pressure differences across the head (Denton and Gray, 1993). This enhanced sensitivity might facilitate the suppression of pressure

Table 2. Morphometrics for the head

Individual	Body length (cm)	Head length (cm)	Head width (cm)	Head height (cm)	a	c	k_1	k_2	H_{morph}
1	9.80	0.87	0.87	1.24	2.01	1.43	0.91	0.43	0.70
2	9.81	0.82	0.94	1.04	1.73	1.10	0.71	0.33	0.61
3	9.60	0.77	0.95	0.99	1.62	1.04	0.66	0.29	0.57
4	9.33	0.80	0.83	1.03	1.95	1.25	0.82	0.40	0.67
5	9.03	0.94	0.94	1.18	2.00	1.25	0.83	0.42	0.68
6	8.65	0.85	0.84	0.99	2.03	1.17	0.80	0.43	0.68
7	8.26	0.81	0.81	0.90	2.01	1.12	0.77	0.42	0.67
Mean	9.21	0.84	0.88	1.05	1.91	1.19	0.78	0.39	0.65
1 s.d.	0.60	0.06	0.06	0.12	0.16	0.13	0.08	0.05	0.05

a, the ratio of head length to head width; c, the ratio of head height to head width, k_1, the first numerical constant; k_2, the second numerical constant; H_{morph}, the predicted index of hydrodynamics

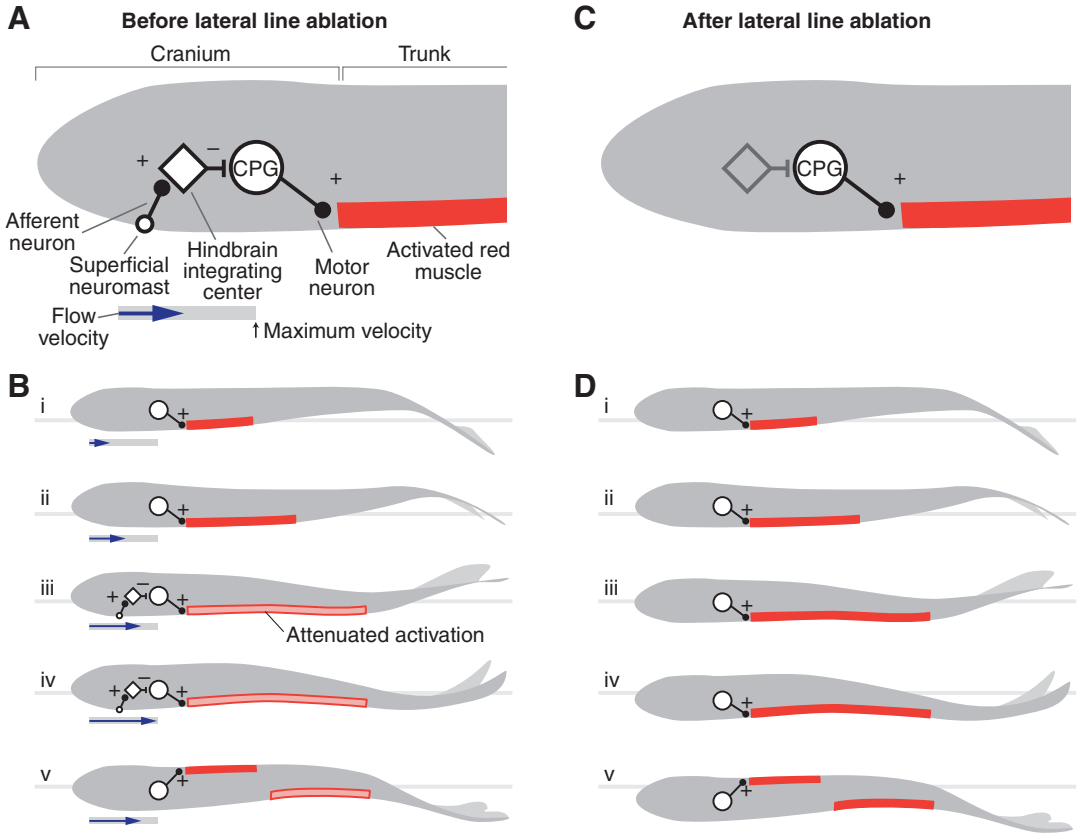

Fig. 7. Hypothetical proportional control system for undulatory swimming. A schematic drawing of a fish (in gray) is shown from a dorsal perspective before (A,B) and after (C,D) lateral line ablation. (A) According to this hypothesis, the afferent signals from superficial neuromasts in the head (denoted by a single white circle) that are stimulated by flow velocity (blue arrow), are integrated within the hindbrain to produce inhibitory signals to the central pattern generator (CPG) that drives the motor patterns for locomotion, which is driven by superficial red muscle (in red). (B) A half tail-beat cycle (i–v) illustrates the pattern of flow, flow sensing, and the motor pattern for locomotion predicted. (i) This cycle begins at the extreme right excursion of the head, when the left anterior muscle is first stimulated by the CPG and the relative flow velocity is low. (ii) As muscle activation propagates, the head translates to the left and the flow velocity increases (Kroese and Schellart, 1992; McHenry et al., 2008; Windsor and McHenry, 2009). (iii) As flow velocity approaches its maximum, the superficial neuromasts transmit an increasingly strong afferent signal that generates an inhibitory signal from the hindbrain to the CPG, which attenuates the magnitude of muscle recruitment (denoted as a pink bar). This inhibition continues as the flow velocity begins to decrease and then the cycle begins for the right side of the body [motor patterns based on Jayne and Lauder (Jayne and Lauder, 1995)]. (C) After lateral line ablation, the superficial neuromasts are removed and no longer generate an inhibitory signal to the CPG. (D) As a consequence, muscle recruitment is maintained at an elevated level throughout the half tail beat and the lateral excursion of the body is consequently greater than before the ablation.

differences to aid in both drag reduction and suppression of flow generated by self-motion.

The golden shiner may not use the lateral line system to minimize drag because the performance advantages are likely minor. The pressure difference across the head is predicted to be greatest when the yaw angle is near its maximum (e.g. Fig. 6A–D). The force generated will be directed normal to the body's surface and the component of this force directed rearward will contribute to drag. For a yaw angle of 3 deg. (typical for a golden shiner, Fig. 5J), the rearward component of the force on the lateral surface of the head would be just 5.2% [equal to sin(3 deg.)] of the total force. Furthermore, surfaces closer to the rostrum are angled forwards and can thereby counter drag generation. Therefore, the great majority of force on the head should not contribute to drag. Furthermore, form drag is generated by pressure differences integrated along the entire length of the body and small kinematic differences at the head may have a negligible influence on this pressure profile. In addition, owing to the small yaw angle, drag generated by pressure is likely to be small relative to that from skin friction on the anterior region of the body. In support of this view, boundary layer measurements demonstrate that the largest stresses that generate skin friction are located in the anterior region (Anderson et al., 2001).

The effect of the lateral line ablation on body undulation

The degree to which the lateral line system affects the lateral amplitude of undulation depends on swimming speed. At the higher speeds considered here (11 and 22 cm s^{-1}), ablating the lateral line system had no apparent effect on swimming kinematics. This negative result may be due to a saturation of lateral line neuromasts at high flow velocities. In support of this interpretation, recordings of afferent lateral line neurons (Engelmann et al., 2000) and their sites of integration in the medulla oblongata (Krother et al., 2002) show that ambient flow of 10 cm s^{-1} is sufficient to interfere with the ability of superficial neuromasts to detect the flow generated by an oscillating sphere (Engelmann et al., 2000). Alternatively, efferent signals to lateral line hair cells may reduce the sensitivity of the lateral line system at faster swimming speeds (Flock and Russell, 1973; Russell and Roberts, 1974), in which case another sensory system, such as the visual system, may compensate for the lack of lateral line feedback.

There are a variety of ways in which the central nervous system (CNS) could integrate lateral line signals to mediate the motor control of swimming. For example, flow detected by the cranial superficial neuromasts could inhibit the central pattern generator (CPG) that initiates the undulatory wave (as detailed in Fig. 7A). This hypothetical proportional control system could be supplemented by a variety of integrative and derivative control mechanisms. Afferent signals from acceleration-sensitive canal neuromasts (van Netten, 2006) could also inhibit motor patterns for derivative control. These hypothetical control systems would require evaluation through a combination of biomechanical and neurophysiological approaches.

In summary, our results support the view that the lateral line system plays a role in the undulatory swimming of some teleost fishes. Contrary to previous studies, our results do not favor the hypothesis that the lateral line system is used to coordinate head motion for active drag reduction (Lighthill, 1995). Instead, ablating the lateral line system caused fish to increase the lateral excursion of undulation when swimming at slow speed ($4.5\,cm\,s^{-1}$). Therefore, the lateral line system appears to provide sensory input to the motor control of the lateral amplitude. Such a control system could allow undulatory swimming to rapidly respond to changes in ambient flow.

ACKNOWLEDGEMENTS

This research was supported by the National Science Foundation through grants to U.K.M. (DBI-0821820) and M.J.M. (IOS-0952344 and IOS-0723288).

REFERENCES

Anderson, E. J., McGillis, W. R. and Grosenbaugh, M. A. (2001). The boundary layer of swimming fish. *J. Exp. Biol.* **204**, 81-102.
Ayali, A., Gelman, S., Tytell, E. D. and Cohen, A. H. (2009). Lateral-line activity during undulatory body motions suggests a feedback link in closed-loop control of sea lamprey swimming. *Can. J. Zool.* **87**, 671-683.
Bainbridge, R. (1963). Caudal fin and body movement in the propulsion of some fish. *J. Exp. Biol.* **40**, 23-56.
Blaxter, J. H. S. and Fuiman, L. A. (1989). Function of the free neuromasts of marine teleost larvae. In *The Mechanosensory Lateral Line: Neurobiology and Evolution* (ed. S. Coombs, P. Gorner and H. Munz), pp. 481-499. New York: Springer-Verlag.
Bleckmann, H. (1994). *Reception of Hydrodynamic Stimuli in Aquatic and Semiaquatic Animals.* Stuttgart: Gustav Fischer.
Collin, S. P. and Shand, J. (2003). Retinal sampling and the visual field in fishes. In *Sensory Processing in Aquatic Environments*, pp. 139-169. New York: Springer-Verlag Inc.
Coombs, S. and Conley, R. A. (1997). Dipole source localization by mottled sculpin.1. Approach strategies. *J. Comp. Physiol. A* **180**, 387-399.
Coombs, S. and Montgomery, J. C. (1999). The enigmatic lateral line system. In *Comparative Hearing: Fish and Amphibians* (ed. R. R. Fay and A. N. Popper), pp. 319-362. New York: Springer-Verlag Inc.
Coombs, S., Hasting, M. and Finneran, J. (1996). Modeling and measuring lateral line excitation patterns to changing dipole source locations. *J. Comp. Physiol. A* **178**, 359-371.
Denton, E. J. and Gray, J. A. B. (1993). Stimulation of the acoustico-lateralis system of clupeid fish by external sources and their own movements. *Philos. Trans. R. Soc. B* **341**, 113-127.
Dijkgraaf, S. (1963). Functioning and significance of lateral-line organs. *Biol. Rev.* **38**, 51-105.
Engelmann, J., Hanke, W., Mogdans, J. and Bleckmann, H. (2000). Hydrodynamic stimuli and the fish lateral line. *Nature* **408**, 51-52.
Flock, A. and Russell, I. J. (1973). Efferent nerve fibres: postsynaptic action on hair cells. *Nat. New Biol.* **16**, 89-91.
Gopalkrishnan, R., Triantafyllou, M. S., Triantafyllou, G. S. and Barrett, D. (1994). Active vorticity control in a shear-flow using a flapping foil. *J. Fluid Mech.* **274**, 1-21.
Harris, J., Cheng, A., Cunningham, L., MacDonald, G., Raible, D. and Rubel, E. (2003). Neomycin-induced hair cell death and rapid regeneration in the lateral line of zebrafish (*Danio rerio*). *J. Assoc. Res. Otolaryngol.* **4**, 219-234.
Jayne, B. C. and Lauder, G. V. (1995). Red muscle motor patterns during steady swimming in largemouth bass: effects of speed and correlations with axial kinematics. *J. Exp. Biol.* **198**, 1575-1587.
Kroese, A. B. A. and Schellart, N. A. M. (1992). Velocity and acceleration-sensitive units in the trunk lateral line of the trout. *J. Neurophys.* **68**, 2212-2221.
Kroese, A. B. A., Das, A. and Hudspeth, A. J. (1989). Blockage of the transduction channels of hair cells in the bullfrog's sacculus by aminoglycoside antibiotics. *Hear. Res.* **37**, 203-218.
Ladich, F. and Bass, A. H. (2003). Underwater sound generation and acoustic reception in fishes with some notes on frogs. In *Sensory Processing in Aquatic Environments* (ed. S. P. Collin and N. J. Marshall), pp. 173-193. New York: Springer-Verlag Inc.
Liao, J. C. (2006). The role of the lateral line and vision on body kinematics and hydrodynamic preference of rainbow trout in turbulent flow. *J. Exp. Biol.* **209**, 4077-4090.
Liao, J. C., Beal, D. N., Lauder, G. V. and Triantafyllou, M. S. (2003a). Fish exploiting vortices decrease muscle activity. *Science* **302**, 1566-1569.
Liao, J. C., Beal, D. N., Lauder, G. V. and Triantafyllou, M. S. (2003b). The Karman gait: novel body kinematics of rainbow trout swimming in a vortex street. *J. Exp. Biol.* **206**, 1059-1073.
Lighthill, J. (1993). Estimates of pressure differences across the head of a swimming clupeid fish. *Philo. Trans. R. Soc. B* **341**, 129-140.
Lighthill, J. (1995). The role of the lateral line in active drag reduction by clupeoid fishes. *Symp. Soc. Exp. Biol.* **49**, 35-48.
McHenry, M. J., Strother, J. A. and van Netten, S. M. (2008). The boundary layer and fluid-structure interaction in the superficial neuromast of the fish lateral line system. *J. Comp. Physiol. A* **194**, 795-810.
McHenry, M. J., Feitl, K. E., Strother, J. A. and Van Trump, W. J. (2009). Larval zebrafish rapidly sense the water flow of a predator's strike. *Biol. Ltrs.* **5**, 477-497.
Montgomery, J., Baker, C. and Carton, A. (1997). The lateral line can mediate rheotaxis in fish. *Nature* **389**, 960-963.
Murakami, S. L., Cunningham, L. L., Werner, L. A., Bauer, E., Pujol, R., Raible, D. W. and Rubel, E. W. (2003). Developmental differences in susceptibility to neomycin-induced hair cell death in the lateral line neuromasts of zebrafish (*Danio rerio*). *Hear. Res.* **186**, 47-56.
Platt, C. (1988). Equilibrium in the vertebrates: signals, sense and steering underwater. In *Sensory Biology of Aquatic Animals* (ed. J. Atema, R. R. Fay, A. N. Popper and W. N. Tavolga), pp. 783-809. New York: Springer-Verlag.
Rowe, D. M., Denton, E. J. and Batty, R. S. (1993). Head turning in herring and some other fish. *Philos. Trans. R. Soc. Lond. B* **341**, 141-148.
Russ, J. C. (1999). *The Image Processing Handbook.* Boca Raton, FL: CRC Press.
Russell, I. J. and Roberts, B. L. (1974). Active reduction of lateral-line sensitivity in swimming dogfish. *J. Comp. Physiol.* **94**, 7-15.
Valentincic, T. (2004). Taste and olfactory stimuli and behavior in fishes. In *The Senses of Fish: Adaptations for the Reception of Natural Stimuli* (ed. G. V. D. Emde, J. Mogdans and B. G. Kapoor), pp. 91-108. Boston: Kluwer Academic Publishers.
van Netten, S. (2006). Hydrodynamic detection by cupulae in a lateral line canal: functional relations between physics and physiology. *Biol. Cybern.* **94**, 67-85.
Videler, J. J. and Hess, F. (1984). Fast continuous swimming of two pelagic predators, saithe (*Pollachius virens*) and mackerel (*Scomber scombrus*): a kinematic analysis. *J. Exp. Biol.* **109**, 209-228.
Williams, S. E., Zenner, H. P. and Schacht, J. (1987). Three molecular steps of aminoglycoside ototoxicity demonstrated in outer hair-cells. *Hear. Res.* **30**, 11-18.
Windsor, S. P. and McHenry, M. J. (2009). The influence of viscous hydrodynamics on the fish lateral-line system. *Integr. Comp. Biol.* **49**, 691-701.